© 2020. Published by The Company of Biologists Ltd | Development (2020) 147, dev194738. doi:10.1242/dev.194738

RESEARCH ARTICLE

The second pharyngeal pouch is generated by dynamic remodeling of endodermal epithelium in zebrafish

Kazunori Okada[1,2] and Shinji Takada[1,2,3,*]

ABSTRACT

Pharyngeal arches (PAs) are segmented by endodermal outpocketings called pharyngeal pouches (PPs). Anterior and posterior PAs appear to be generated by different mechanisms, but it is unclear how the anterior and posterior PAs combine. Here, we addressed this issue with precise live imaging of PP development and cell tracing of pharyngeal endoderm in zebrafish embryos. We found that two endodermal bulges are initially generated in the future second PP (PP2) region, which separates anterior and posterior PAs. Subsequently, epithelial remodeling causes contact between these two bulges, resulting in the formation of mature PP2 with a bilayered morphology. The rostral and caudal bulges develop into the operculum and gill, respectively. Development of the caudal PP2 and more posterior PPs is affected by impaired retinoic acid signaling or *pax1a*/*b* dysfunction, suggesting that the rostral front of posterior PA development corresponds to the caudal PP2. Our study clarifies an aspect of PA development that is essential for generation of a seamless array of PAs in zebrafish.

KEY WORDS: Pharyngeal arch, Pharyngeal pouch, Endoderm, Operculum, Epithelial remodeling, Segmentation

INTRODUCTION

Elaborate morphological features of organisms can often be explained by simple metameric motifs that are transiently established during vertebrate development (Carroll, 1995; Hannibal and Patel, 2013). For instance, conspicuous segmental structures called pharyngeal arches (PAs) are bilaterally arranged in the ventral region of the head (Fig. 1A) (Graham, 2001; Graham and Richardson, 2012). PAs give rise to the segmental organization of skeletons, muscles, nerves and vessels in the pharynx; therefore, specification and segmentation of PAs are crucial for development of the vertebrate head (Graham and Smith, 2001). The most anterior PA, referred to as PA1 or the mandibular arch (MA), forms the jaw. The second anterior PA, PA2, also called the hyoid arch (HA), generates the hyoid. In addition, the more posterior PAs, known as the branchial arches (BAs), give rise to many pharyngeal derivatives, including the thymus and parathyroid glands. Tripartite streams of cranial neural crest cells (CNCCs), referred to as the trigeminal, hyoid and branchial streams, contribute to PA1, PA2 and the BAs, respectively (Graham et al., 2004; Hunt et al., 1991; Lumsden et al., 1991; Schilling and Kimmel, 1994; Serbedzija et al., 1992). However, segmentation of PA units occurs independently of these CNCCs (Gavalas et al., 2001; Veitch et al., 1999). Rather, pharyngeal endoderm contributes to this segmentation by generating epithelial outpocketings called pharyngeal pouches (PPs), which physically define the anterior and posterior interfaces of each PA (Graham and Richardson, 2012; Graham and Smith, 2001). Each PP lies flat along the antero-posterior axis and consists of two layers of epithelial sheet.

The two most anterior PAs (MA and HA) are likely to have different characteristics from the posterior PAs (BAs). The anterior PAs express genes involved in myogenesis and chondrogenesis, whereas the posterior PAs do not undergo myogenesis and chondrogenesis in chick or mouse embryos (Poopalasundaram et al., 2019). Several other genes also exhibit anterior- and posterior-specific expression in pharyngeal ectoderm. For instance, the expression of sonic hedgehog (Shh) is excluded or highly reduced in posterior pouches in chicks and mice, and Shh signaling prevents *Gcm2* expression in the first and second pharyngeal endoderm (Ankamreddy et al., 2019; Grevellec et al., 2011). In addition, expression of several Dlx genes is specific for anterior PAs in chick and mouse embryos (Poopalasundaram et al., 2019). Interestingly, the anterior PAs are segmented simultaneously, whereas the posterior PAs (BAs) are generated sequentially in anterior to posterior order (Crump et al., 2004a; Graham et al., 2014; Veitch et al., 1999), suggesting discrete regulation of anterior and posterior PA segmentation. Correspondingly, retinoic acid (RA) deficiency in zebrafish (Kopinke et al., 2006), quail (Quinlan et al., 2002), rat (White et al., 1998) and mouse (Wendling et al., 2000) embryos consistently results in abnormalities in segmentation of the third and more posterior PAs. Similarly, *pax1* knockout medaka (Okada et al., 2016) and *Ripply3* knockout mice (Okubo et al., 2011) show loss of BAs, but normal MAs and HAs. These studies suggest that distinct segmentation mechanisms for anterior and posterior PAs might cooperate to establish the entire series of PAs. However, development of this complex PA segmentation has been poorly understood. Especially puzzling has been the question of how the seamless array of PAs is generated from anterior and posterior PAs, which are formed by different mechanisms.

Recent studies of zebrafish PP development have revealed the dynamic cellular nature of the endoderm in forming PPs (Choe et al., 2013; Choe and Crump, 2014, 2015a,b), highlighting the advantages of the zebrafish model to dissect processes of PP development. In this study, we examined development of zebrafish pharyngeal endoderm, especially focusing on the formation of PP2, which is located at the boundary between the anterior and posterior PAs. Precise examination by live-imaging and cell-tracing experiments performed in zebrafish showed that PP2 is formed in an unexpected manner. Rostral and caudal edges of PP2 are initially formed separately, then subsequently establish contact through

[1]Exploratory Research Center on Life and Living Systems, National Institutes of Natural Sciences, 5-1 Higashiyama, Myodaijicho, Okazaki 444-8787, Japan. [2]National Institute for Basic Biology, National Institutes of Natural Sciences, 5-1 Higashiyama, Myodaiji-cho, Okazaki 444-8787, Japan. [3]Department for Basic Biology, SOKENDAI (The Graduate University for Advanced Studies), 5-1 Higashiyama, Myodaiji-cho, Okazaki 444-8787, Japan.

*Author for correspondence (stakada@nibb.ac.jp)

K.O., 0000-0002-6180-661X; S.T., 0000-0003-4125-6056

Handling Editor: Steve Wilson
Received 17 July 2020; Accepted 28 October 2020

Development (2020) 147, dev194738. doi:10.1242/dev.194738

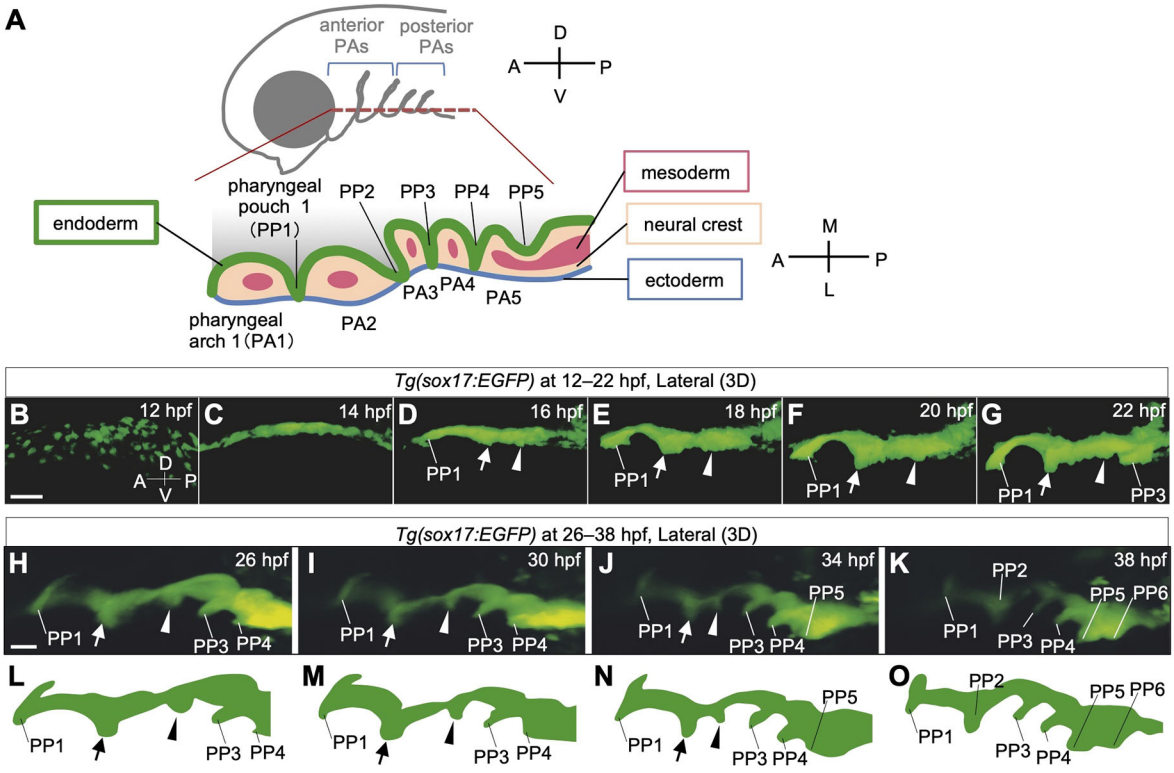

Fig. 1. Time-lapse observations of pharyngeal endoderm during PP segmentation in *Tg(sox17:EGFP)* zebrafish embryos. (A) Schematic of the bilateral arrangement of PAs in the ventral region of the head. (B-K) Time-lapse analysis of the pharyngeal endoderm of *Tg(sox17:EGFP)* zebrafish from 12 hpf to 22 hpf (B-G, Movie 1) and from 26 hpf to 38 hpf (H-K, Movie 2). Rostral (arrows) and caudal (arrowheads) bulges appeared posterior to PP1 and gradually fused to form PP2. (L-O) Schematic illustrations of the shape of the lateral pharyngeal endoderm in H-K, respectively. A, anterior; D, dorsal; L, lateral; M, medial; P, posterior; PA1-5, the first to fifth pharyngeal arch; PP1-6, the first to sixth pharyngeal pouches; V, ventral. Scale bars: 50 µm (B) and 20 µm (H).

dynamic remodeling of endoderm epithelium, and finally form a mature PP bilayer.

RESULTS

Dynamic epithelial remodeling in PP2 formation during zebrafish embryogenesis

To better understand the development of pharyngeal endoderm, we performed time-lapse imaging of endodermal cells in transgenic zebrafish, *Tg(sox17:EGFP)*, in which EGFP expression was specifically driven in endodermal cells by the *sox17* promoter (Mizoguchi et al., 2008). PP1 appeared at 16 h post-fertilization (hpf; Fig. 1B-D, Movie 1), whereas PP outpocketings, including PP3 and more posterior PPs, were generated sequentially from anterior to posterior after 16 hpf (Fig. 1E-K, Movie 2). Unexpectedly, we found that two endodermal bulges appeared at ∼16 hpf, with PP1 budding in the area where PP2 would be generated (Fig. 1D, Movie 1). Notably, these bulges were gradually remodeled and finally merged to form a bilayered PP2 (Fig. 1H-O, Movie 2). This remodeling occurred not prior to, but during, sequential generation of posterior PPs, and the two bulges were finally merged at the time when PP6 was formed (Fig. 1K). These findings strongly suggest that mature, bilayered PP2 is formed approximately after the formation of most posterior PPs (Fig. 1H-O, Movie 2).

To understand the dynamics of the endodermal bulges, we performed a lineage-tracing experiment by means of endoderm-specific photoconversion. To this end, we created *Tg(sox17:Kaede)*, a transgenic line harboring *Kaede* expression under control of the *sox17* promoter. Photoconversion of cells in the rostral bulge at 20 hpf revealed that these cells contributed to the rostral layer of PP2 at 48 hpf (Fig. 2A-E and Fig. S1). Descendants of these cells spread extensively to form the inner lining of the distal part of the HA, where an opercular flap would later expand (Fig. 2A-E and Fig. S1). By contrast, descendants from the caudal bulge became distributed in the caudal layer of PP2 at 48 hpf, especially its proximal region (Fig. 2F-J and Fig. S1). In addition, cells in the intermediate region between the rostral and caudal bulges contributed to the more distal and ventral regions of the caudal layer and the dorsal edge of PP2 (Fig. 2K-N and Fig. S1). Based on patterns of cell traces (n=29, Fig. 2 and Fig. S1), we outlined fates of endodermal cells in the future PP2 region at 20 hpf (Fig. 2O). In summary, PP2 was generated by dynamic remodeling of endodermal cells between the rostral and the caudal bulges, which directly contributed to respective rostral and caudal layers of PP2.

Rostral and caudal bulges of the future PP2 endoderm region exhibit characteristics of the PP

Our time-lapse observations and cell-tracing experiments revealed that PP2 arose from two distinct endodermal domains, which then coalesced into a pouch structure via dynamic remodeling of the endoderm. To understand development of PP2 more precisely, we examined expression of PP-specific genes in the future PP2 endoderm. First, we examined expression of *nkx2.3*, which is observed in both rostral and caudal compartments of all zebrafish PPs (Lee et al., 1996). Expression of *nkx2.3* was initially evident at 20 hpf. At this stage, *nkx2.3* expression was detected not only in PP1 but also in the rostral and caudal bulges of PP2 (Fig. 3A-D and Fig. S2). Whereas *nkx2.3* expression in these areas appeared simultaneously (Fig. S2A), *nkx2.3* expression corresponding to

Development (2020) 147, dev194738. doi:10.1242/dev.194738

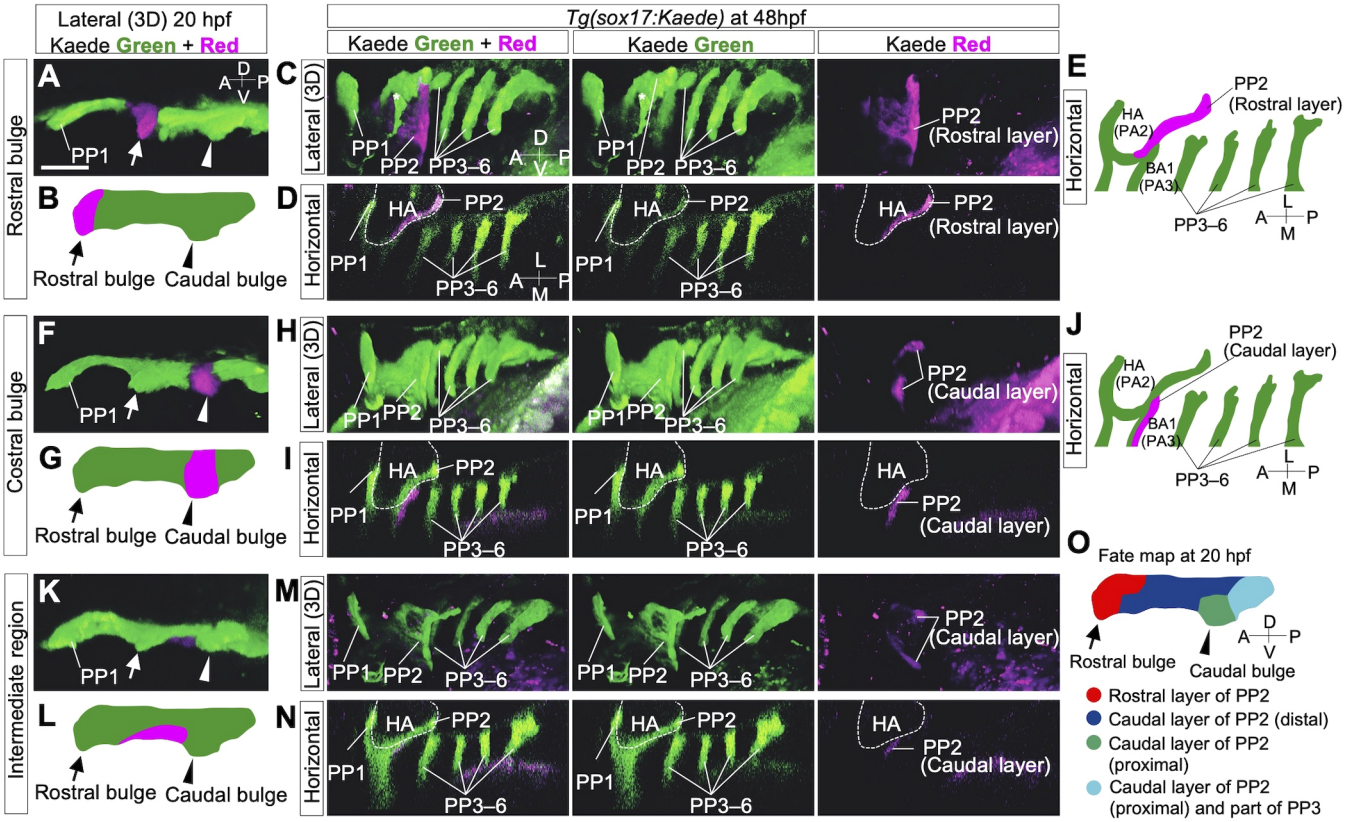

Fig. 2. Lineage tracing of endodermal cells in *Tg(sox17:Kaede)* zebrafish embryos by photoconversion. (A-E) Cells of the rostral bulge (arrows) were marked at 20 hpf (A,B). At 48 hpf, cells of the rostral bulge contributed to the large area of the rostral portion of PP2 (C-E). (F-J) The cells of the caudal bulge (arrowheads) were marked at 20 hpf (F,G). At 48 hpf, the descendant cells contributed to the caudal region of PP2 rather proximally (H-J). (K-N) The cells of the intermediate domain of a putative PP2 (between the rostral and caudal bulges) were marked (K,L). At 48 hpf, these descendants composed the dorsally and ventrally distant area in the caudal part of PP2 (M,N). (O) Overview of the cell fate of future PP2 endoderm at 20 hpf. Cell fates were examined in various regions of the presumptive PP2 endoderm by photoconversion (n=29, A-N and Fig. S1); these are summarized, showing the dynamic reorganization of the endoderm forming PP2. A, anterior; BA, branchial arch; D, dorsal; HA, hyoid arch; L, lateral; M, medial; P, posterior; PP1-6, the first to sixth pharyngeal pouches; V, ventral. The asterisk indicates a blood vessel. The positions of the HA (dashed lines) were identified by the surrounding *sox17*-positive endoderm. Scale bar: 50 µm.

posterior PPs (PP3 and PP4) appeared gradually with sequential segmentation of the posterior PPs (Fig. S2B,C). Thus, *nkx2.3* expression was detected in a temporal sequence similar to the progression of PA morphogenesis observed by time-lapse imaging (Fig. 1B-K, Movie 1). Consistent with PP2 maturation, *nkx2.3*-positive rostral and caudal bulges gradually converged to form PP2 (Fig. S2A-C). We also examined expression of *pax1b*, which is expressed in PPs of many vertebrates. Like *nkx2.3*, *pax1b* was expressed in all PPs. Furthermore, its expression was detected in the future PP2 ectoderm, including in the rostral and caudal bulges (Fig. S2D). These expression patterns of PP-specific genes suggest that at least some characteristics of PP2 were already present in the future PP2 ectoderm, including in the bulges. Furthermore, the separate expression of *nkx2.3* in the two distinct bulges supports results obtained by time-lapse observations and cell-tracing experiments, showing that PP2 was formed by complex remodeling of the two distinct endodermal domains.

To further understand development of the future PP2 endoderm, we next examined rostral and caudal layer-specific molecular characteristics. We found that expression of *tbx1* was specific to the rostral layer of each PP in normal embryos up to 30 hpf, whereas that of *fgf3* was specific to the caudal layer of each PP (Fig. S2E-H). Interestingly, even at the beginning of PP2 development, expression of *tbx1* was strongly detected in the rostral bulge, but not in the caudal bulge (Fig. 3E-H), and that of *fgf3* was the opposite (Fig. 3E,F,I,J). This result strongly suggests that the rostral and caudal bulges have already acquired distinct rostrocaudal characteristics prior to epithelial remodeling to form PP2. In other words, immature PP2 first appeared as a wide and abnormally shaped epithelial sheet, including both rostral and caudal domains, and is subsequently remodeled into bilayered epithelium. We refer to these rostral and caudal bulges as R2 and C2, respectively, hereafter (Fig. 3K).

R2 and C2 contribute independently to skeletal development in HA and BA

Because molecular characteristics of the rostral and caudal layers of PP2 were observed in the endodermal domains of R2 and C2, respectively, we next investigated whether rostral and caudal identities had actually been determined in R2 and C2. We specifically ablated endodermal cells in the R2 or C2 region using infrared laser-mediated heating (Kamei et al., 2009; Zeng et al., 2016). To visualize endodermal cells, we used *Tg(sox17:EGFP)* embryos in this laser-ablation experiment.

Consistent with results from cell-lineage tracing, ablation of R2 cells at 20 hpf (Fig. 4A,A′) impaired expansion of the rostral region of PP2 at 48 hpf (n=3/3, Fig. 4B,C). In later stages, R2 ablation resulted in loss of HA-derived dermal bones of branchiostegal rays (BR; n=12/16) and the opercular (OP; n=10/16), which together compose the operculum (Fig. 4D-F). This ablation occasionally reduced the size of other HA-derived skeletal structures, such as the hyomandibular (HM; n=3/16)

Development (2020) 147, dev194738. doi:10.1242/dev.194738

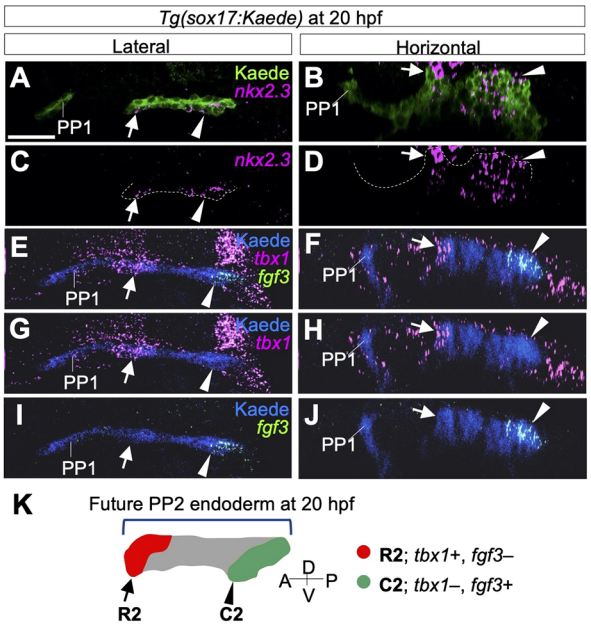

Fig. 3. Separate formations and rostrocaudal identity of PP2 endoderm at 20 hpf. (A-D) Separate expression of *nkx2.3* indicated the rostral (arrows) and caudal (arrowheads) bulges of PP2 endoderm identified immunohistochemically with the anti-Kaede antibody. (E-J) Expression of *tbx1* (E-H) and *fgf3* (E,F,I,J) was detected in rostral (arrows) and caudal (arrowheads) bulges of PP2, showing early specification of the rostrocaudal polarity of PP2. (K) According to fate analysis and molecular profiles, the rostral and the caudal bulges of the future PP2 are distinctly defined as R2 (red, arrow) and C2 (green, arrowhead), respectively. Whereas cells of the intermediate region (gray) contribute to the caudal region, *fgf3*, a caudal marker, is not expressed in these cells at 20 hpf. A, anterior; D, dorsal; P, posterior; PP1, the first pharyngeal pouch; V, ventral. Scale bar: 20 µm. Four embryos were analyzed for *nkx2.3* expression and three embryos for *tbx1* and *fgf3* expression.

and ceratohyal (CH; *n*=6/16) cartilages, but ceratobranchial (CB) cartilages, which are derived from BAs, were completely normal (*n*=16/16, Fig. 4D, Fig. S3C). For operculum development, Shh expression is required in the HA (Richardson et al., 2012). We found that *shha* was expressed in endoderm corresponding to R2-derived cells (Fig. 4G,H), and that this expression was reduced (*n*=5/12) or eliminated (*n*=5/12) by R2 ablation (Fig. 4I), suggesting that the R2 region gives rise to a signaling center of Shh for operculum formation. In contrast to R2, ablation of cells in the C2 region (Fig. 4J,J′) caused abnormalities in the proximo-caudal PP2 adjacent to BA1 (or PA3; *n*=3/3, Fig. 4K,L), resulting in specific loss of the first CB cartilage (CB1; *n*=8/8, Fig. 4M). However, ablation of cells between R2 and C2 (Fig. 4N,N′) did not cause any loss of the pharyngeal skeleton, although the position of CB1 on the ablation side shifted posteriorly and laterally (*n*=4/6, Fig. 4Q). Interestingly, this ablation caused a split of endoderm between HA and BA1 (*n*=10/12, Fig. 4O,P), which were almost normally formed, showing the requirement of intermediate endoderm for integration of HA and BA1. Loss of skeletal elements does not appear to result from deficits in CNCCs caused by infrared irradiation of the endodermal cells, because PA mesenchymal cells and expression of *dlx2a*, which is a credible marker of CNCCs in PAs, were not affected by ablation of adjacent endoderm (*n*=6, Fig. S3A,B). Therefore, we conclude that endodermal cells of R2, C2 and the intermediate region serve distinct functions in craniofacial development in zebrafish. Significantly, those functions were determined in endodermal domains prior to remodeling for morphological maturation of PP2.

Distinct molecular machineries for rostral and caudal development of PP2

Previous studies suggested that development of anterior and posterior PAs appears to occur via distinct molecular mechanisms (Kopinke et al., 2006; Okada et al., 2016; Okubo et al., 2011; Quinlan et al., 2002; Wendling et al., 2000; White et al., 1998). These studies suggest that a mechanistic boundary between them might exist around PP2. Because our findings enabled us to dissect developmental processes of PP2 into rostral and caudal events, we next addressed the issue of how separate molecular mechanisms could coordinate to produce PP2.

As RA signaling is specifically required for development of the posterior PPs (Kopinke et al., 2006; Quinlan et al., 2002; Wendling et al., 2000; White et al., 1998), we supposed that the R2–C2 boundary would correspond to the anterior border of RA function. Visualization of RA activity utilizing a transgenic fish *Tg(RARE:Venus)*, which harbors a Venus reporter driven by RA-responsive elements (RARE) (Retnoaji et al., 2014), showed that Venus was expressed in C2 cells at 20 hpf and persisted in their descendants, as well as in posterior pharyngeal endoderm (Fig. 5A-F). By contrast, Venus expression was never detected in R2 and PP1 endoderm during our examination (Fig. 5A-F). Furthermore, treatment with *N*,*N*-diethylaminobenzaldehyde (DEAB), which inhibits RA biosynthesis, impaired C2 formation and *fgf3* expression in C2 (Fig. 5K-N). By contrast, this treatment did not cause an obvious change in *tbx1* expression in R2 (Fig. 5G-J). Thus, RA signaling was specifically activated in and required for pharyngeal endoderm posterior to R2, indicating that the anterior border of RA function actually corresponded to the R2–C2 border we had identified.

Our previous study also showed that *pax1* is specifically required for the development of posterior PPs in medaka (Okada et al., 2016). Zebrafish has two *pax1* homologs, *pax1a* and *pax1b*; therefore, we generated double-knockout (DKO) mutants of these genes (referred to as *pax1* DKO) by performing CRISPR/Cas9-mediated mutagenesis (Fig. S4). As expected, *pax1* DKO embryos showed definite abnormalities in development of their PPs posterior to C2, but not in R2 (Fig. 6A-D). Consistently, gill skeletons, but not opercular skeletons, were lost in *pax1* DKO larvae (Fig. 6E-H). The anterior part of the HM (aHM), in which PP1 is required developmentally (Crump et al., 2004b), was lost in *pax1* DKO larvae (Fig. 6E-H), although PP1 was normally formed in mutant embryos (Fig. 6A-D). Thus, *pax1a/b* genes appear to participate in aHM development at a later stage after PP1 formation, but this role apparently differs from their role in PP development posterior to C2.

The membrane protein, Alcam, accumulates in PP epithelium to stabilize bilayered PP morphology (Choe et al., 2013). Similar to RA and *pax1a/b*, we found that its accumulation was low in PP1 and R2, but high in C2 and more posterior PPs (Fig. 7). This result suggests that the R2–C2 border might also have separated the morphogenetic process of endodermal epithelial cells. Taken together, we conclude that two distinct developmental processes occur in pharyngeal endoderm either anterior or posterior to the R2–C2 border, and that these processes subsequently merge to form zebrafish PP2.

DISCUSSION

Generally, segmentation in animal development occurs in a simultaneous manner, as in *Drosophila* germ-band formation (Davis and Patel, 2002), or in a sequential manner, as represented by vertebrate somitogenesis (Pourquié, 2011). Interestingly, PA segmentation is thought to be achieved by a peculiar combination of these distinct styles. The anterior PAs, i.e. MA and HA, are

Development (2020) 147, dev194738. doi:10.1242/dev.194738

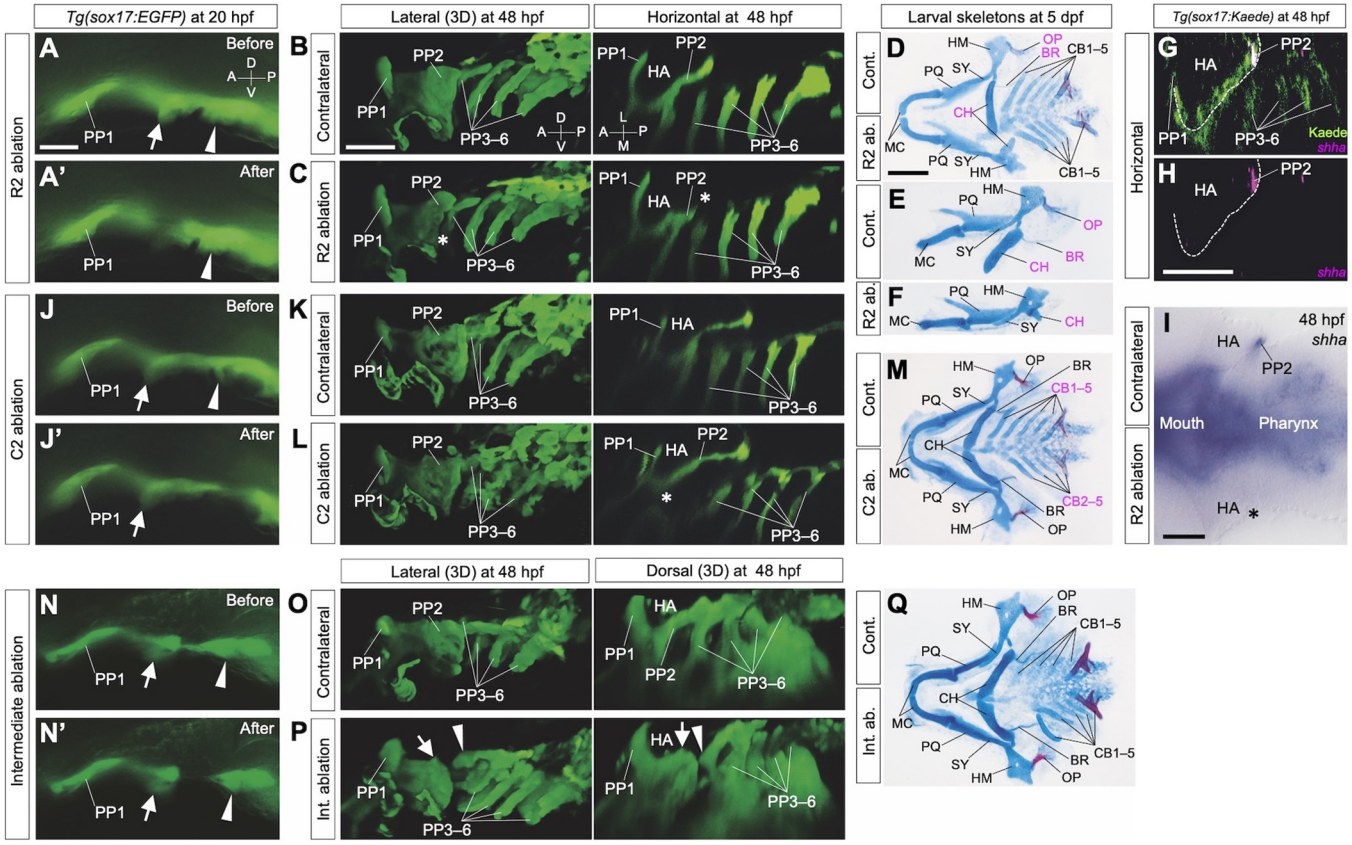

Fig. 4. Early determination of distinct roles for later skeletal patterns in R2 and C2 endoderm. (A,A′) Cells of R2 (arrows) in *Tg(sox17:EGFP)* embryos were ablated at 20 hpf. (B-F) R2 ablation caused a specific loss of epithelial expansion of the caudal lining of the HA (asterisks in C; *n*=3/3) and reductions in HA-derived skeletal elements, especially in the opercular series (D-F; OP, *n*=10/16; BR, *n*=12/16). In addition, this ablation occasionally caused a size reduction in other HA-derived skeletal structures, such as the HM (Fig. S3C; *n*=3/16) and CH (D-F; *n*=6/16). (G,H) Expression of *shha*, required for opercular development, was detected in PP2 endoderm occupied by R2 descendants. (I) Consistent with endodermal (B,C) and the skeletal (D-F) phenotypes, R2 ablation caused a specific loss of *shha* expression in PP2, as shown in a flat-mounted embryo (asterisk in I; *n*=12). (J,J′) Cells of C2 (arrowheads) in *Tg(sox17:EGFP)* embryos were ablated at 20 hpf. (K-M) Ablation of C2 cells resulted in loss of the proximal region of PP2, which consists of the rostral lining of the third PA (BA1) (K,L, asterisk in L; *n*=3/3), resulting in loss of CB1 cartilage (M; *n*= 8/8). (N,N′) Endodermal cells between R2 (arrows) and C2 (arrowheads) were ablated in *Tg(sox17:EGFP)* embryos at 20 hpf. (O-Q) Ablation of cells in the intermediate region did not affect segregation of HA and BA1 but caused abnormal arrangements of them, shown by a split between HA and BA1 (O,P; *n*=10/12). Correspondingly, on the ablated sides, the positions of BA1-derived CB1 cartilage shifted posteriorly, although a complete set of the pharyngeal structures developed (Q; *n*=4/6). Images of ablated sides (C,F,L,Q) are inverted in a left-right direction for comparisons with contralateral sides. A, anterior; BR, branchiostegal ray; CB1-5, the first to fifth ceratobranchials; CH, ceratohyal cartilages; D, dorsal; HA, hyoid arch; HM, hyomandibular; L, lateral; M, medial; MC, Meckel's cartilage; OP, opercular bone; P, posterior; PP1-6, the first to sixth pharyngeal pouches; PQ, palatoquadrate; SY, symplectic; V, ventral. Scale bars: 20 µm (A), 50 µm (B,H,I) and 100 µm (D).

segmented simultaneously, whereas the posterior PAs (BAs) are generated sequentially in anterior to posterior order (Crump et al., 2004a; Graham et al., 2014; Veitch et al., 1999). However, a developmental process employing a combined segmentation system has never been reported. Zebrafish PA development, in which dynamic epithelial remodeling of the endoderm occurs, is a good model to resolve development of the vertebrate head (Choe et al., 2013; Choe and Crump, 2014, 2015a,b). In this study, by using precise live imaging in zebrafish, we found that the bilayered morphology of PP2, the border between the anterior and posterior PAs, was established by dynamic remodeling of the endoderm after generation of both anterior and posterior PAs. Given that anterior and posterior PAs are formed independently, this endodermal remodeling appears to be essential to merge anterior and posterior PAs, resulting in formation of a seamless array of PAs in zebrafish.

Our cell-tracing experiments in endoderm clearly revealed that the two endoderm bulges R2 and C2, which appear in the future PP2 endoderm region, directly contribute to the rostral and caudal layers of PP2, respectively. The rostral or caudal identity of each bulge had already been determined prior to PP2 formation, as evidenced by gene expression and cell-ablation experiments. However, intermediate endodermal cells between R2 and C2 did not contribute to the formation of PA-derived skeletons, although they were required for a tight arrangement of anterior and posterior PAs. These results suggest that the identity of rostral or caudal layers of PP is specified prior to formation of bilayered pouch morphology, at least in the case of PP2.

Based on our results, we propose a novel mode of vertebrate PA development. That is, HA and BAs are established independently by distinct developmental mechanisms. Accordingly, posterior PA-specific defects and PP2 insufficiency, which are commonly reported as phenotypes of RA-deficient vertebrates (Kopinke et al., 2006; Quinlan et al., 2002; Wendling et al., 2000; White et al., 1998), are more reasonably explained as defects occurring posterior to C2. Similarly, PA development in *pax1* mutants of teleost fish (Okada et al., 2016) and *Ripply3* mutant mice (Okubo et al., 2011) appears to be impaired posterior to C2 endoderm. By contrast, *tbx1* is required not only for posterior PA development, but also for HA development

Development (2020) 147, dev194738. doi:10.1242/dev.194738

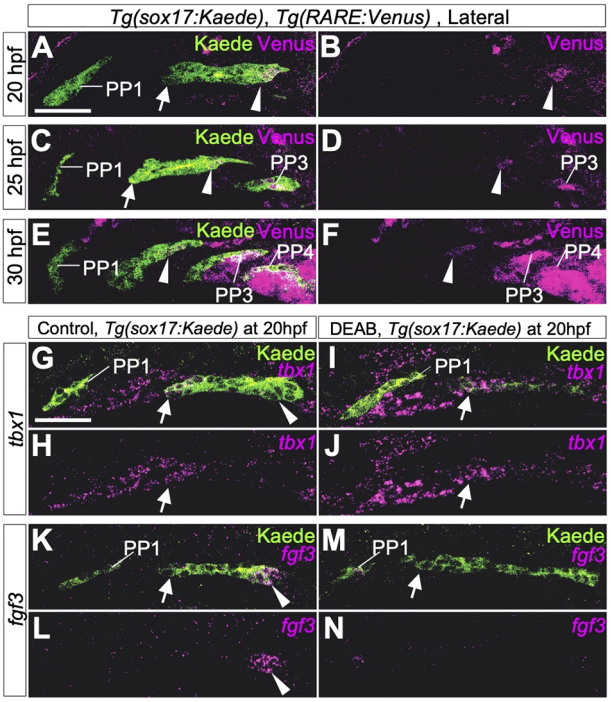

Fig. 5. Boundaries of molecular mechanisms forming PPs between the rostral and caudal portions of PP2. (A-F) Immunohistochemistry of double transgenic embryos of *Tg(sox17:Kaede)* and *Tg(RARE:Venus)* showed specific signals of the RA reporter Venus in the caudal part of PP2 and in posterior PPs but not in the rostral edge of PP2 and PP1 endoderm at 20 hpf (A,B), 25 hpf (C,D) and 30 hpf (E,F). Three embryos were analyzed at each time point. (G-N) Expression of *tbx1* (magenta in G-J) or *fgf3* (magenta in K-N) in control (G,H,K,L) and DEAB-treated transgenic (I,J,M,N) embryos carrying *sox17:Kaede* R2 (arrows) at 20 hpf. Expression of *tbx1* was not affected in DEAB-treated embryos (G,J, indicated by arrows). By contrast, RA deficiency caused by DEAB treatment resulted in loss of *fgf3* expression in C2 (K-N, indicated by arrowheads). Owing to the angle at which images were taken, the size and morphology of each PP appear to be slightly different in each confocal plane, but, in these experiments, DEAB treatment did not cause major anomalies in morphology of PP1 or PP2. More than five embryos were used for each experiment.

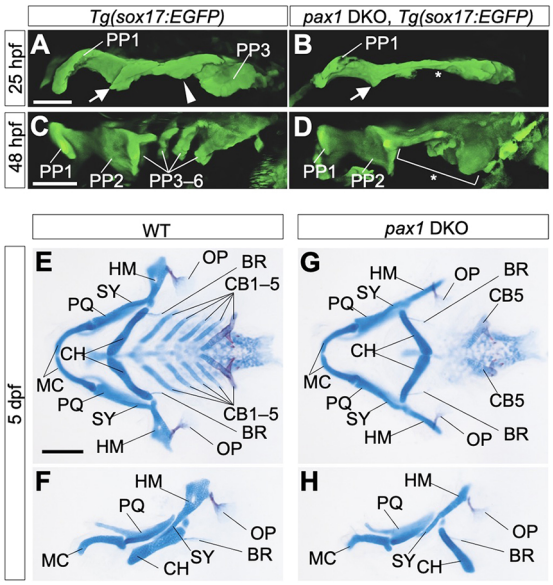

Fig. 6. Pharyngeal abnormalities in *pax1* dKO mutant embryos. (A-D) Endodermal morphologies of wild-type (A,C) and *pax1a; pax1b* double-knockout (*pax1* DKO) embryos (B,D) harboring a *Tg(sox17:EGFP)* transgene. At 25 hpf, PP1, R2, C2 and PP3 were formed in the wild type (A), but, in *pax1* DKO embryos, C2 and PP3 were specifically defective (B, asterisk). At 48 hpf, complete segments of PP were observed in the wild type (C), whereas caudal PP2 and more posterior PPs were not formed in *pax1* DKO embryos (D, bracket and asterisk). Notably, PP1 and the rostral part of PP2 were almost normal in the mutants (D). All pictures show the left side of the pharyngeal region. PP1-6, the first to sixth pharyngeal pouches. Arrows indicate R2; arrowheads indicate C2. Scale bars: 50 µm. (E-H) Flat-mount views of pharyngeal skeletons (E,G) and left-side views of MA- and HA-derived skeletal elements (F,H) in wild-type (E,F) and *pax1* DKO (G,H) larvae at 5 days post-fertilization (dpf). CB1-4 and the anterior part of the HM were lost, although OP and BR were normally formed in *pax1* DKO larvae (G,H). BR, branchiostegal ray; CB1-5, the first to fifth ceratobranchials; CH, ceratohyal; HM, hyomandibular; MC, Meckel's cartilage; OP, opercular bone; PQ, palatoquadrate; SY, symplectic. Scale bars: 100 µm. Three embryos were used for endoderm observation and five embryos were used for skeletal analysis.

(Jerome and Papaioannou, 2001). However, *tbx1* expression is independent of *pax1* function in HA endoderm, but not in BA endoderm (Okada et al., 2016). Thus, the regulatory system of *tbx1* expression is spatially consistent with our idea, and suggests that there are distinct gene regulatory networks between anterior and posterior PAs. It is also an interesting question as to whether Hox genes are involved in the anterior- or posterior-specific mechanism in endoderm development. In chick embryos, *Hoxa3* expression transiently extends through PP2, whereas mouse *Hoxa3* is expressed in PP3 and PP4, but not PP2 (Gordon, 2018). In zebrafish, *hoxa3a* and *hoxb3a* are expressed in posterior PAs (Hogan et al., 2004), but it is uncertain whether Hox paralogs are involved in the regulatory network specific to posterior PAs.

What is the significance of the specifically modified PP morphogenesis at PP2, in terms of morphological evolution of the vertebrate head? We suppose that this modification probably contributed to evolution of the opercular system, which is conserved in osteichthyans (Richardson et al., 2012). A recent study on a fossilized placoderm, *Entelognathus*, which has opercular and BRs, suggests that the osteichthyan-like pharyngeal system existed in stem gnathostomes (Zhu et al., 2013). Furthermore, it has also been suggested that the chondrichthyan affinity of acanthodians, which possess a hyoidean gill cover with BRs, implies unique evolution of the chondrichthyan pharyngeal system composed of septal gills (Brazeau and de Winter, 2015; Brazeau and Friedman, 2015; Janvier, 1996). Although skeletal elements of the operculum have been lost during tetrapod evolution, the embryonic opercular flap, which is derived from the Shh-expressing HA, encloses the posterior pharyngeal region during amniote development (Graham and Richardson, 2012; Richardson et al., 2012). In this study, we found that R2 endoderm contributes directly to the operculum, including Shh-expressing cells in the zebrafish HA. Thus, we propose that HA development, distinct from that of BAs, must have been acquired by stem gnathostomes as the crucial basis for the novel pharyngeal system of the hyoidean operculum, leading to extant osteichthyans.

It is still unclear how the development of PP1 and the rostral layer of PP2 is regulated. The independence of PP1 development from that of other PPs has been suggested by previous studies on zebrafish (Crump et al., 2004a,b; Talbot et al., 2012) and mouse (Jerome and Papaioannou, 2001; Xu et al., 2005) development. Interestingly, in amphioxus, formation of the first gill slit is less affected by *pax1/9* knockdown than that of other gill slits, which exhibit severe defects (Liu et al., 2015). This finding implies evolutionarily conserved independence of the first endodermal bulge from others. Therefore, development of vertebrate PPs,

Development (2020) 147, dev194738. doi:10.1242/dev.194738

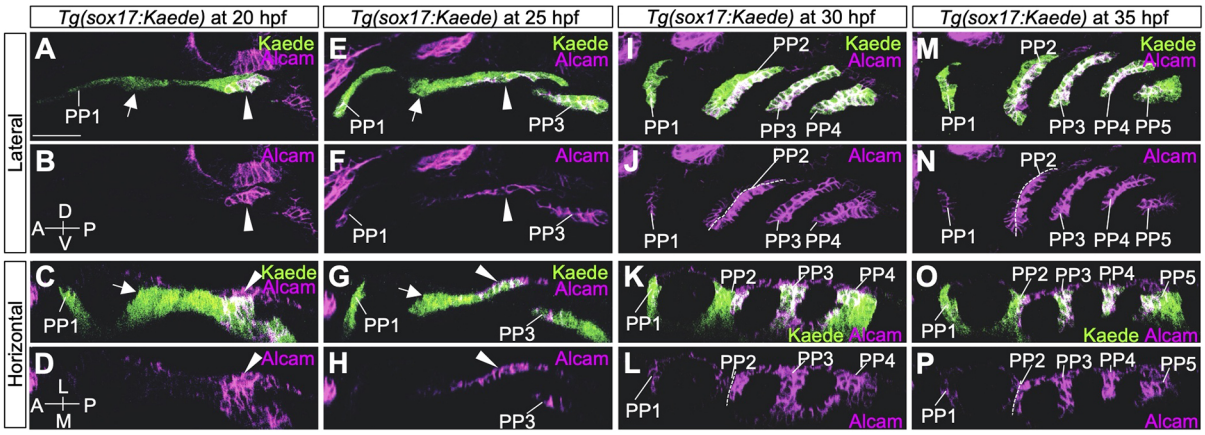

Fig. 7. Expression analysis of Alcam in the PP endoderm of *Tg(sox17:Kaede)*. (A-D) At 20 hpf, strong expression of Alcam was evident in C2 but hardly detected in PP1 and R2 endoderm. (E-H) At 25 hpf, Alcam was high in PP3 and the caudal portion of PP2 but almost absent in PP1 and the rostral part of PP2. (I-L) At 30 hpf, high accumulation of Alcam was detected in PP3, PP4 and the caudal layer of PP2, whereas it was at a very low level in PP1 and the rostral layer of PP2. (M-P) At 35 hpf, high accumulation of Alcam was detected in PP3, PP4, PP5 and the caudal part of PP2, whereas it was at a very low level in PP1 and the rostral layer of PP2. A, anterior; D, dorsal; L, lateral; M, medial; P, posterior; PP1-5, the first to fifth pharyngeal pouches; V, ventral. Arrows indicate R2; arrowheads indicate C2. Scale bar: 50 µm. More than two embryos were analyzed at each time point.

especially in gnathostomes, could be considered as involving three sections: PP1, the rostral layer of PP2 and a more posterior region. Significantly, these endodermal sections correspond to the interfaces of the three streams of CNCCs comprising the MA, HA and BAs. Therefore, we propose that modifications in endodermal segmentation reinforced topological restrictions of neural crest cell streams in the PAs. Further studies on the development of PPs could answer one of the biggest questions regarding development of the vertebrate head, the logic for coordination between pre-patterned neural crest cells and endodermal segmentation.

MATERIALS AND METHODS

Zebrafish embryos

Zebrafish with the TL2 background were used as the wild type, as described previously (Kishimoto et al., 2004). Collected embryos were incubated at 28°C. Embryos that would be fixed later than 25 hpf were treated with 0.003% 1-Phenyl-2-thiourea (PTU) from 10 hpf until fixation to inhibit melanin synthesis. This study was performed in accordance with Guidelines for Animal Experimentation of the National Institutes of Natural Sciences, with approval from its Institutional Animal Care and Use Committee.

Transgenic zebrafish and mutagenesis

Tg(sox17:EGFP) and *Tg(RARE:Venus)* were used in this study. For generation of *Tg(sox17:Kaede)*, the Kaede complementary DNA fragment from pKaede-S1 (MBL) and the same promoter sequence as used for the *Tg(sox17:EGFP)* were combined and cloned into the pSK-tol2B vector (Yabe and Takada, 2012). Transgenesis was performed using the Tol2 system (Kawakami et al., 2004). For CRISPR/Cas9-mediated knockout, target sequences were determined using the ZiFiT Targeter (Sander et al., 2010). Construction of guide RNA vectors and preparation of single-guide RNA (sgRNA) and Cas9 mRNA were performed as described previously (Cong et al., 2013; Hwang et al., 2013). Mutation efficiency was assessed by performing a T7 endonuclease assay (Chen et al., 2012) with the following primers: 5′-TTGATTTAGGTCATGTGTGTTATATG-3′, 5′-TTTGTTTGT-AGTCCCGTATGTTTTT-3′ for *pax1a* and 5′-GTTTTTCTGACAATG-CAAAAAGTG-3′, 5′-CGTATTTCCCAAGCAAATATCC-3′ for *pax1b*. Details on *pax1a* and *pax1b* mutagenesis and sequences of sgRNAs are provided in Fig. S4. For microinjections, 1 nl of each injection solution (Tol2 transgenesis: 25 ng/µl plasmid, 50 ng/µl Tol2 mRNA, 0.2 M KCl and 0.05% Phenol Red; CRISPR/Cas9: 25 ng/µl sgRNA, 100 ng/µl Cas9 mRNA, 0.2 M KCl and 0.05% Phenol Red) were injected into one-cell-stage zebrafish embryos using an IM300 micro injector (Narishige).

Imaging

Living embryos of *Tg(sox17:EGFP)*, from which chorions had been manually removed, were anesthetized with 0.02% ethyl-3-aminobenzoate methanesulfonate (MS-222) in 1/3 zebrafish Ringer's solution. For observations with a Leica SP8, embryos were moved to mounting medium (0.15% low-melting-point agarose, 0.02% MS-222, 0.003% PTU in 1/3 zebrafish Ringer's solution) and individually set in the medium on a glass-bottomed dish. Embryos were manually positioned using a tungsten needle with an eyelash on its tip. *Z*-stack images were taken at 10-min intervals, and stack images were processed with an LAS X (Leica) to make 3D images, optical sections and movies. For imaging with a Zeiss Lightsheet Z.1, anesthetized embryos were mounted as previously described (Weber et al., 2014). Images taken at 10-min intervals were processed with ZEN Black (Zeiss) and subsequently with Imaris (Bitplane) to make movies.

Photoconversion and cell ablation

Embryos of *Tg(sox17:Kaede)* for photoconversion or *Tg(sox17:EGFP)* for cell ablation were mounted as described above. Photoconversion was performed with a Leica SP8 using a 405-nm diode laser. Regions of interest (ROIs) in Kaede-expressing endoderm at 20 hpf were converted using the ROI tool in LAS X (Leica). Converted embryos were released from the gel and incubated at 28°C, and were observed again at 48 hpf. Cell ablation with an infrared laser-evoked gene operator (IR-LEGO) system (Sigmakoki IR-LEGO 1000, Sigma Koki) was performed as previously described (Zeng et al., 2016). High-power flash irradiation with an infrared laser (80 mW for 8 ms) was performed several times until EGFP signals of target regions had been eliminated. Ablated embryos were released from the gel and incubated at 28°C until subsequent experiments could be performed. For cell ablation controls, *Tg(sox17:EGFP)* embryos were injected with mRNA of histone H2A-mCherry at the one-cell stage to visualize the cell nucleus in the live condition. At 20 hpf, embryos were scanned with a Nikon A1 before ablation and moved to the IR-LEGO. After infrared irradiation on the IR-LEGO, embryos were immediately moved to the Nikon A1 and scanned again to evaluate off-target damage to cells of adjacent PAs. This procedure was repeated, and ablated embryos were fixed in 4% paraformaldehyde and stored in methanol at −20°C for *in situ* hybridization with a *dlx2a* probe, and for immunohistochemistry with anti-GFP antibody, to assess CNCCs in the PA.

In situ hybridization and immunostaining

Whole-mount *in situ* hybridization of zebrafish was performed as described previously (Jowett, 2001). For double-fluorescence *in situ* hybridization experiments, anti-DIG-POD (Roche) and anti-FITC-POD (Roche) were used to detect each hapten in RNA probes. Fluorescent signals were detected with a

TSA Plus Cy3/fluorescein system (PerkinElmer). Plasmids for probes of *dlx2a*, *nkx2.3* and *shha* (Krauss et al., 1993) were kindly donated by Drs M. Hibi, Y. Kikuchi and S. Krauss, respectively. Primers for cloning other probes of zebrafish genes were as follows: 5′-ATGCTTTCGTGTTTTGCAGAGCAAACATAC-3′, 5′-TTACGAGGATGAGGTAGAAAGGCTGAGTCC-3′ for *pax1a*; 5′-ATGCAAATGGATCAGACGTACGGGGAGGTG-3′, 5′-TTATGAGTCTGAGAGTCCATGAACAGCGCT-3′ for *pax1b*; 5′-ATGATTTCAGCAATATCAAGCCCGTGGCTG-3′, 5′-TTATCTGGGTCCGTAGTCATAATTAGTCGG-3′ for *tbx1*; and 5′-AAATCTCACGATAGGCTCCCTG-3′, 5′-AAAGTACTCCTGATTGCAGT-3′ for *fgf3*. Immunostaining was conducted as previously reported (Yabe et al., 2016) using primary antibodies anti-Alcam (1:500; Developmental Studies Hybridoma Bank, University of Iowa, USA), anti-Kaede (1:400; MBL, PM012), anti-GFP (1:400; Abcam, ab13970), followed by Alexa Fluor-conjugated secondary antibodies (Invitrogen). Bone and cartilage staining of zebrafish larvae was performed as previously described (Walker and Kimmel, 2007). Rehydrated embryos were treated with RNaseA and subsequently stained overnight at room temperature with YOYO1-Iodide in PBST (1:2000; Thermo Fisher Scientific). Stained embryos were rinsed with PBST several times, dehydrated with methanol and soaked in benzyl alcohol/benzyl benzoate (1:2 ratio) prior to confocal imaging.

DEAB treatment

DEAB stock, which was stored at −20°C, was prepared at 100 mM in dimethyl sulfoxide (DMSO). DEAB treatment was conducted at final concentrations of 10^{-4} M for zebrafish (from 10 hpf to 20 hpf), as previously described (Kopinke et al., 2006). Embryos were cultured in a dark incubator, at 28°C. Control embryos were treated under the same conditions, but with 0.1% DMSO only.

Acknowledgements

We thank Dr Hiroshi Wada for helpful suggestions on the manuscript. Many other individuals contributed to make this study possible and we gratefully acknowledge their support: Dr Yutaka Kikuchi provided *Tg(sox17:EGFP)* zebrafish, a plasmid of the *sox17* promoter and the *nkx2.3* probe; Dr Shin-ichi Higashijima provided technical support for CRISPR/Cas9 technology; Dr Stefan Krauss kindly provided the *shha* probe; Ms Hideko Utsumi offered technical support; and Mrs Kayoko Takashiro maintained the zebrafish. Staff members in the Spectrography and Bioimaging Facility, National Institute for Basic Biology Core Research Facilities provided technical support. All members of the Takada laboratory contributed helpful discussions. We thank Dr Steven D. Aird for editing the manuscript.

Competing interests

The authors declare no competing or financial interests.

Author contributions

Conceptualization: K.O., S.T.; Methodology: K.O.; Formal analysis: K.O.; Investigation: K.O.; Writing - original draft: K.O., S.T.; Writing - review & editing: K.O., S.T.; Visualization: K.O.; Supervision: S.T.; Project administration: S.T.; Funding acquisition: S.T.

Funding

This work was supported by the following programs: Grants-in-Aid for Scientific Research (B) (23370094 and 18H02454 to S.T.) and Grants-in-Aid for Scientific Research on Innovative Areas (24111002, 17H05782 and 19H04797 to S.T.) from the Japan Society for the Promotion of Science. Additional support came from grants from the National Institutes of Natural Sciences (NINS Joint Research Program to S.T.).

Supplementary information

Supplementary information available online at
https://dev.biologists.org/lookup/doi/10.1242/dev.194738.supplemental

References

Ankamreddy, H., Min, H., Kim, J. Y., Yang, X., Cho, E. S., Kim, U. K. and Bok, J. (2019). Region-specific endodermal signals direct neural crest cells to form the three middle ear ossicles. *Development* **146**, dev167965. doi:10.1242/dev.167965

Brazeau, M. D. and de Winter, V. (2015). The hyoid arch and braincase anatomy of Acanthodes support chondrichthyan affinity of 'acanthodians'. *Proc. R. Soc. B* **282**, 20152210. doi:10.1098/rspb.2015.2210

Brazeau, M. D. and Friedman, M. (2015). The origin and early phylogenetic history of jawed vertebrates. *Nature* **520**, 490-497. doi:10.1038/nature14438

Carroll, S. B. (1995). Homeotic genes and the evolution of arthropods and chordates. *Nature* **376**, 479-485. doi:10.1038/376479a0

Chen, J., Zhang, X., Wang, T., Li, Z., Guan, G. and Hong, Y. (2012). Efficient detection, quantification and enrichment of subtle allelic alterations. *DNA Res.* **19**, 423-433. doi:10.1093/dnares/dss023

Choe, C. P. and Crump, J. G. (2014). Tbx1 controls the morphogenesis of pharyngeal pouch epithelia through mesodermal Wnt11r and Fgf8a. *Development* **141**, 3583-3593. doi:10.1242/dev.111740

Choe, C. P. and Crump, J. G. (2015a). Dynamic epithelia of the developing vertebrate face. *Curr. Opin. Genet. Dev.* **32**, 66-72. doi:10.1016/j.gde.2015.02.003

Choe, C. P. and Crump, J. G. (2015b). Eph-Pak2a signaling regulates branching of the pharyngeal endoderm by inhibiting late-stage epithelial dynamics. *Development* **142**, 1089-1094. doi:10.1242/dev.115774

Choe, C. P., Collazo, A., Trinh, L. A., Pan, L., Moens, C. B. and Crump, J. G. (2013). Wnt-dependent epithelial transitions drive pharyngeal pouch formation. *Dev. Cell* **24**, 296-309. doi:10.1016/j.devcel.2012.12.003

Cong, L., Ran, F. A., Cox, D., Lin, S., Barretto, R., Habib, N., Hsu, P. D., Wu, X., Jiang, W., Marraffini, L. A. et al. (2013). Multiplex genome engineering using CRISPR/Cas systems. *Science* **339**, 819-823. doi:10.1126/science.1231143

Crump, J. G., Maves, L., Lawson, N. D., Weinstein, B. M. and Kimmel, C. B. (2004a). An essential role for Fgfs in endodermal pouch formation influences later craniofacial skeletal patterning. *Development* **131**, 5703-5716. doi:10.1242/dev.01444

Crump, J. G., Swartz, M. E. and Kimmel, C. B. (2004b). An integrin-dependent role of pouch endoderm in hyoid cartilage development. *PLoS Biol.* **2**, e244. doi:10.1371/journal.pbio.0020244

Davis, G. K. and Patel, N. H. (2002). Short, long, and beyond: molecular and embryological approaches to insect segmentation. *Annu. Rev. Entomol.* **47**, 669-699. doi:10.1146/annurev.ento.47.091201.145251

Gavalas, A., Trainor, P., Ariza-McNaughton, L. and Krumlauf, R. (2001). Synergy between Hoxa1 and Hoxb1: the relationship between arch patterning and the generation of cranial neural crest. *Development* **128**, 3017-3027.

Gordon, J. (2018). Hox genes in the pharyngeal region: how Hoxa3 controls early embryonic development of the pharyngeal organs. *Int. J. Dev. Biol.* **62**, 775-783. doi:10.1387/ijdb.180284jg

Graham, A. (2001). The development and evolution of the pharyngeal arches. *J. Anat.* **199**, 133-141. doi:10.1046/j.1469-7580.2001.19910133.x

Graham, A. and Richardson, J. (2012). Developmental and evolutionary origins of the pharyngeal apparatus. *EvoDevo* **3**, 24. doi:10.1186/2041-9139-3-24

Graham, A. and Smith, A. (2001). Patterning the pharyngeal arches. *BioEssays* **23**, 54-61. doi:10.1002/1521-1878(200101)23:1<54::AID-BIES1007>3.0.CO;2-5

Graham, A., Begbie, J. and McGonnell, I. (2004). Significance of the cranial neural crest. *Dev. Dyn.* **229**, 5-13. doi:10.1002/dvdy.10442

Graham, A., Butts, T., Lumsden, A. and Kiecker, C. (2014). What can vertebrates tell us about segmentation? *EvoDevo* **5**, 24. doi:10.1186/2041-9139-5-24

Grevellec, A., Graham, A. and Tucker, A. S. (2011). Shh signalling restricts the expression of Gcm2 and controls the position of the developing parathyroids. *Dev. Biol.* **353**, 194-205. doi:10.1016/j.ydbio.2011.02.012

Hannibal, R. L. and Patel, N. H. (2013). What is a segment? *EvoDevo* **4**, 35. doi:10.1186/2041-9139-4-35

Hogan, B. M., Hunter, M. P., Oates, A. C., Crowhurst, M. O., Hall, N. E., Heath, J. K., Prince, V. E. and Lieschke, G. J. (2004). Zebrafish gcm2 is required for gill filament budding from pharyngeal ectoderm. *Dev. Biol.* **276**, 508-522. doi:10.1016/j.ydbio.2004.09.018

Hunt, P., Gulisano, M., Cook, M., Sham, M.-H., Faiella, A., Wilkinson, D., Boncinelli, E. and Krumlauf, R. (1991). A distinct Hox code for the branchial region of the vertebrate head. *Nature* **353**, 861-864. doi:10.1038/353861a0

Hwang, W. Y., Fu, Y., Reyon, D., Maeder, M. L., Tsai, S. Q., Sander, J. D., Peterson, R. T., Yeh, J.-R. and Joung, J. K. (2013). Efficient genome editing in zebrafish using a CRISPR-Cas system. *Nat. Biotechnol.* **31**, 227-229. doi:10.1038/nbt.2501

Janvier, P. (1996). *Early Vertebrates*. Oxford, UK: Clarendon Press.

Jerome, L. A. and Papaioannou, V. E. (2001). DiGeorge syndrome phenotype in mice mutant for the T-box gene, Tbx1. *Nat. Genet.* **27**, 286-291. doi:10.1038/85845

Jowett, T. (2001). Double in situ hybridization techniques in zebrafish. *Methods* **23**, 345-358. doi:10.1006/meth.2000.1147

Kamei, Y., Suzuki, M., Watanabe, K., Fujimori, K., Kawasaki, T., Deguchi, T., Yoneda, Y., Todo, T., Takagi, S., Funatsu, T. et al. (2009). Infrared laser-mediated gene induction in targeted single cells in vivo. *Nat. Methods* **6**, 79-81. doi:10.1038/nmeth.1278

Kawakami, K., Takeda, H., Kawakami, N., Kobayashi, M., Matsuda, N. and Mishina, M. (2004). A transposon-mediated gene trap approach identifies developmentally regulated genes in zebrafish. *Dev. Cell* **7**, 133-144. doi:10.1016/j.devcel.2004.06.005

Kishimoto, Y., Koshida, S., Furutani-Seiki, M. and Kondoh, H. (2004). Zebrafish maternal-effect mutations causing cytokinesis defect without affecting mitosis or equatorial vasa deposition. *Mech. Dev.* **121**, 79-89. doi:10.1016/j.mod.2003.10.001

Kopinke, D., Sasine, J., Swift, J., Stephens, W. Z. and Piotrowski, T. (2006). Retinoic acid is required for endodermal pouch morphogenesis and not for pharyngeal endoderm specification. *Dev. Dyn.* **235**, 2695-2709. doi:10.1002/dvdy.20905

Krauss, S., Concordet, J.-P. and Ingham, P. W. (1993). A functionally conserved homolog of the Drosophila segment polarity gene hh is expressed in tissues with polarizing activity in zebrafish embryos. *Cell* **75**, 1431-1444. doi:10.1016/0092-8674(93)90628-4

Lee, K.-H., Xu, Q. and Breitbart, R. E. (1996). A new tinman-related gene, nkx2.7, anticipates the expression of nkx2.5 and nkx2.3 in zebrafish heart and pharyngeal endoderm. *Dev. Biol.* **180**, 722-731. doi:10.1006/dbio.1996.0341

Liu, X., Li, G. and Wang, Y.-Q. (2015). The role of the Pax1/9 gene in the early development of amphioxus pharyngeal gill slits. *J. Exp. Zoo.l B Mol. Dev. Evol.* **324**, 30-40. doi:10.1002/jez.b.22596

Lumsden, A., Sprawson, N. and Graham, A. (1991). Segmental origin and migration of neural crest cells in the hindbrain region of the chick embryo. *Development* **113**, 1281-1291.

Mizoguchi, T., Verkade, H., Heath, J. K., Kuroiwa, A. and Kikuchi, Y. (2008). Sdf1/Cxcr4 signaling controls the dorsal migration of endodermal cells during zebrafish gastrulation. *Development* **135**, 2521-2529. doi:10.1242/dev.020107

Okada, K., Inohaya, K., Mise, T., Kudo, A., Takada, S. and Wada, H. (2016). Reiterative expression of pax1 directs pharyngeal pouch segmentation in medaka. *Development* **143**, 1800-1810. doi:10.1242/dev.130039

Okubo, T., Kawamura, A., Takahashi, J., Yagi, H., Morishima, M., Matsuoka, R. and Takada, S. (2011). Ripply3, a Tbx1 repressor, is required for development of the pharyngeal apparatus and its derivatives in mice. *Development* **138**, 339-348. doi:10.1242/dev.054056

Poopalasundaram, S., Richardson, J., Scott, A., Donovan, A., Liu, K. and Graham, A. (2019). Diminution of pharyngeal segmentation and the evolution of the amniotes. *Zoological Lett.* **5**, 6. doi:10.1186/s40851-019-0123-5

Pourquié, O. (2011). Vertebrate segmentation: from cyclic gene networks to scoliosis. *Cell* **145**, 650-663. doi:10.1016/j.cell.2011.05.011

Quinlan, R., Gale, E., Maden, M. and Graham, A. (2002). Deficits in the posterior pharyngeal endoderm in the absence of retinoids. *Dev. Dyn.* **225**, 54-60. doi:10.1002/dvdy.10137

Retnoaji, B., Akiyama, R., Matta, T., Bessho, Y. and Matsui, T. (2014). Retinoic acid controls proper head-to-trunk linkage in zebrafish by regulating an anteroposterior somitogenetic rate difference. *Development* **141**, 158-165. doi:10.1242/dev.097568

Richardson, J., Shono, T., Okabe, M. and Graham, A. (2012). The presence of an embryonic opercular flap in amniotes. *Proc. R. Soc. B* **279**, 224-229. doi:10.1098/rspb.2011.0740

Sander, J. D., Maeder, M. L., Reyon, D., Voytas, D. F., Joung, J. K. and Dobbs, D. (2010). ZiFiT (Zinc Finger Targeter): an updated zinc finger engineering tool. *Nucleic Acids Res.* **38**, W462-W468. doi:10.1093/nar/gkq319

Schilling, T. F. and Kimmel, C. B. (1994). Segment and cell type lineage restrictions during pharyngeal arch development in the zebrafish embryo. *Development* **120**, 483-494.

Serbedzija, G. N., Bronner-Fraser, M. and Fraser, S. E. (1992). Vital dye analysis of cranial neural crest cell migration in the mouse embryo. *Development* **116**, 297-307.

Talbot, J. C., Walker, M. B., Carney, T. J., Huycke, T. R., Yan, Y.-L., BreMiller, R. A., Gai, L., Delaurier, A., Postlethwait, J. H., Hammerschmidt, M. et al. (2012). fras1 shapes endodermal pouch 1 and stabilizes zebrafish pharyngeal skeletal development. *Development* **139**, 2804-2813. doi:10.1242/dev.074906

Veitch, E., Begbie, J., Schilling, T. F., Smith, M. M. and Graham, A. (1999). Pharyngeal arch patterning in the absence of neural crest. *Curr. Biol.* **9**, 1481-1484. doi:10.1016/S0960-9822(00)80118-9

Walker, M. B. and Kimmel, C. B. (2007). A two-color acid-free cartilage and bone stain for zebrafish larvae. *Biotech. Histochem.* **82**, 23-28. doi:10.1080/10520290701333558

Weber, M., Mickoleit, M. and Huisken, J. (2014). Multilayer mounting for long-term light sheet microscopy of zebrafish. *J. Vis. Exp.* e51119. doi:10.3791/51119

Wendling, O., Dennefeld, C., Chambon, P. and Mark, M. (2000). Retinoid signaling is essential for patterning the endoderm of the third and fourth pharyngeal arches. *Development* **127**, 1553-1562.

White, J. C., Shankar, V. N., Highland, M., Epstein, M. L., DeLuca, H. F. and Clagett-Dame, M. (1998). Defects in embryonic hindbrain development and fetal resorption resulting from vitamin A deficiency in the rat are prevented by feeding pharmacological levels of all-trans-retinoic acid. *Proc. Natl. Acad. Sci. USA* **95**, 13459-13464. doi:10.1073/pnas.95.23.13459

Xu, H., Cerrato, F. and Baldini, A. (2005). Timed mutation and cell-fate mapping reveal reiterated roles of Tbx1 during embryogenesis, and a crucial function during segmentation of the pharyngeal system via regulation of endoderm expansion. *Development* **132**, 4387-4395. doi:10.1242/dev.02018

Yabe, T. and Takada, S. (2012). Mesogenin causes embryonic mesoderm progenitors to differentiate during development of zebrafish tail somites. *Dev. Biol.* **370**, 213-222. doi:10.1016/j.ydbio.2012.07.029

Yabe, T., Hoshijima, K., Yamamoto, T. and Takada, S. (2016). Quadruple zebrafish mutant reveals different roles of Mesp genes in somite segmentation between mouse and zebrafish. *Development* **143**, 2842-2852. doi:10.1242/dev.133173

Zeng, C.-W., Kamei, Y., Wang, C.-T. and Tsai, H.-J. (2016). Subtypes of hypoxia-responsive cells differentiate into neurons in spinal cord of zebrafish embryos after hypoxic stress. *Biol. Cell* **108**, 357-377. doi:10.1111/boc.201600015

Zhu, M., Yu, X., Ahlberg, P. E., Choo, B., Lu, J., Qiao, T., Qu, Q., Zhao, W., Jia, L., Blom, H. et al. (2013). A Silurian placoderm with osteichthyan-like marginal jaw bones. *Nature* **502**, 188-193. doi:10.1038/nature12617